CrossMark

ORIGINAL PAPER

Non-linear Compensated Dwell Time for Efficient Fused Silica Surface Figuring Using Inductively Coupled Plasma

Zuocai Dai[1,2] · Xuhui Xie[1,2] · Heng Chen[1,2] · Lin Zhou[1,2]

Abstract Atmospheric plasma etching has been increasingly applied in the fabrication of optical elements for high efficiency and near-zero damage to optical surfaces. However, the non-linearity of material removal rate is inevitable because of the thermal effect of inductively coupled plasma (ICP) etching for fused silica. To apply ICP to figure fused silica surface, the time-varying non-linearity between material removal rate and dwell time is analyzed. An experimental model of removal function is established considering the time-varying non-linearity. According to this model, an algorithm based on nested pulsed iterative method is proposed for calculating and compensating this time-varying non-linearity by varying the dwell time. Simulation results show that this algorithm can calculate and adjust the dwell time accurately and remove surface errors with rapid convergence. Surface figuring experiments were set up on the fused silica planar work-pieces with a size of 100 mm (width) × 100 mm (length) × 10 mm (thickness). With the compensated dwell time, the surface error converges rapidly from 4.556 λ PV (peak-to-valley) to 0.839 λ PV within 13.2 min in one iterative figuring. The power spectral density analysis indicates that the spatial frequency errors between 0.01 and 0.04 mm^{-1} are smoothed efficiently, and the spatial frequency errors between 0.04 and 0.972 mm^{-1} are also corrected. Experimental results demonstrate that the ICP surface figuring can achieve high convergence for surface error reduction using the compensated dwell time. Therefore, the ICP surface figuring can greatly improve surface quality and machining efficiency for fused silica optical elements.

Keywords Inductively coupled plasma · Fused silica · Material removal rate · Time-varying non-linearity · Surface figuring

✉ Zuocai Dai
daizuocai@163.com

1 College of Mechatronics Engineering and Automation, National University of Defense Technology, Changsha 410073, China

2 Hu'nan Key Laboratory of Ultra-precision Machining Technology, Changsha 410073, China

Introduction

Fused silica materials have found an increasingly wide utilization in optical systems, such as inertial confinement fusion, large telescope, microelectronics and aerospace, for their chemical stability, UV permeability, and radiation resistance and high laser damage threshold [1]. Currently, the universal machining processes of fused silica optical elements are grinding, lapping and polishing [2]. However, all these methods inevitably result in deformation, residual stress and surface damage on the optical surface because of their mechanical contact material removal feature [3]. Because the application performance requirement is increasingly raised for fused silica, it needs a new ultra-smooth surface machining method to produce a better machined surface [4]. At present, the classic ultra-smooth surface machining methods include bath polishing, float polishing, magnetorheological polishing, ion beam figuring, elastic emission processing etc. Although the methods are able to produce a smoothed surface, their efficiency cannot meet the needs of efficient machining for fused silica optical elements. Therefore atmospheric plasma etching has been proposed for fused silica optical elements fabrication as an efficient machining method [5].

In the atmospheric plasma etching process, the basic material removal principle is that active fluorine atoms chemically react with the silica atoms to generate SiF_4 gas to realize material removal in atmospheric environment. In this process, the active fluorine atoms are ionized from fluorine rich gases like SF_6, CF_4 or NF_3 by plasma source. This process method is called the atmospheric plasma material etching. Since atmospheric plasma etching process is a chemical etch to realize material removal, it is a non-surface damage and high efficient non-contact process method without vacuum condition, which is able to process aspheric and free-form optical elements. Therefore, many research institutes have studied atmospheric plasma machining technology [6].

Osaka University in Japan developed a plasma chemical vaporization machining (PCVM) using capacitive coupling plasma (CCP). Its achievement of material removal efficiency is equivalent to that of the precision grinding for machining fused silica optical elements [7, 8]. IOM Institute in Germany applied CCP to silicon carbide surface figuring by designing a plasma jet process called plasma jet machining (PJM) [9]. To improve the material removal rate of PJM, a microwave plasma source is developed to replace the conventional radio frequency plasma source [10, 11]. By this means, the PJM's material removal rate for fused silica machining was improved from the lowest 0.002 mm^3/min up to 44 mm^3/min, which shows the good potential of atmospheric plasma etch process for the optical elements machining [12]. Harbin Institute of Technology in China also developed a coaxial electrode type plasma source using CCP, which is called atmospheric pressure plasma processing (APPP). The APPP has two processing modes, jet mode and contact discharge mode. The material removal efficiency of contact discharge processing mode for fused silica is much higher than that of jet processing mode [15]. Cranfield University in Britain used ICP to develop reactive atom plasma technology (RAPT) for ULE machining which could give a very high material removal rate and very low surface roughness [13, 14]. Our research group developed arc-enhanced plasma machining technology (AEPM) for silicon carbide efficient machining using ICP [17, 18].

Although ICP method has high material removal efficiency and produces near-zero damage on optical surfaces, there still exist some problems needed to be solved, such as the thermal problem. During ICP machining for fused silica surface, it generates a lot of thermal energy, which leads to high temperature on the machined surface. This high and

varying temperature leads to non-linear variation of the material remove rate, which seriously affects the ability to obtain the required surface profile for fused silica work-pieces [19–22]. Since the ICP machining is a chemical reactive etching, which is directly influenced by the etching surface temperature, especially for insulating substrates, this problem is made more serious by low thermal conductivity. This leads to a significant non-linear removal behavior as dwell time of plasma increases because of consequently strong local heating. In order to find out the relation between the etching surface temperature and material removal rate, researchers have applied simulation methods [6, 22, 24]. In 2011, Johannes Meister et al. developed a process simulation model considering spatio-temporal variations of surface temperature and temperature-related material removal performance, which could predict the processed work-piece topography [22]. This simulation model could instruct PJM to realize a real deterministic process. However, its shortcoming is that the simulation procedure requires a long computing time of about 16–20 h. So, it is not convenient to be used to iteratively calculate dwell time directly. In 2012, Castelli et al. proposed a tool-path algorithm involving a reversed staggered raster which considered a thermal compensatory coefficient [6]. This algorithm could effectively restrict the thermal effect on the material removal rate during ICP surface figuring for fused silica, gaining a rapid convergence and decreasing the residual errors to λ/40 RMS. However, the thermal compensatory coefficient and the choice of the targeted percentage of the material removal used an empirical approach. Therefore, it is still necessary to explore a more convenient method.

In this paper, to compensate non-linearity of material removal rate caused by the thermal effect during the plasma etching process, the time-varying non-linearity between material removal rate and dwell time is firstly analyzed in detail. Then the algorithm based on NPIM is proposed for calculating and compensating the time-varying nonlinear relationship with the dwell time. Specifically, this algorithm only needs to apply the time-varying non-linearity of material removal rate to the nested pulsed iterative calculation, which is more convenient to calculate and compensate the dwell time for fused silica surface figuring. The simulation results demonstrate that surface error quickly converges from 4.556 λ PV to 0.776 λ PV on 100 mm × 100 mm × 10 mm fused silica work-piece. The experimental surface figuring results further verify this algorithm with the surface error converged from 4.556 λ PV to 0.839 λ PV within 13.2 min for this work-piece. Both of the simulation results and the experimental surface figuring results confirm the use-fulness of the algorithm, which demonstrates that ICP surface figuring can be performed with rapid surface error convergence for efficient machining of fused silica.

Form assessment of surfaces was performed by means of vertical interferometer, while the surface temperature distribution during surface figuring was characterized through the Fluke thermal imager (FLUKE-TI400) and the subsurface damage defects were measured by digital microscope (VHX-600).

## Experimental Model of Removal Function and Discussion

In ICP machining, a prerequisite to applying ICP to optical surface figuring is to acquire an accurate material removal model, a so-called experimental model of the removal function. It is known that the removal function is closely dependent on the structure of plasma source. Figure 1a shows the nested composite structure of the plasma source with included inner, intermediate and outer three layer pipe tubes. In this structure, the exit of outer tube
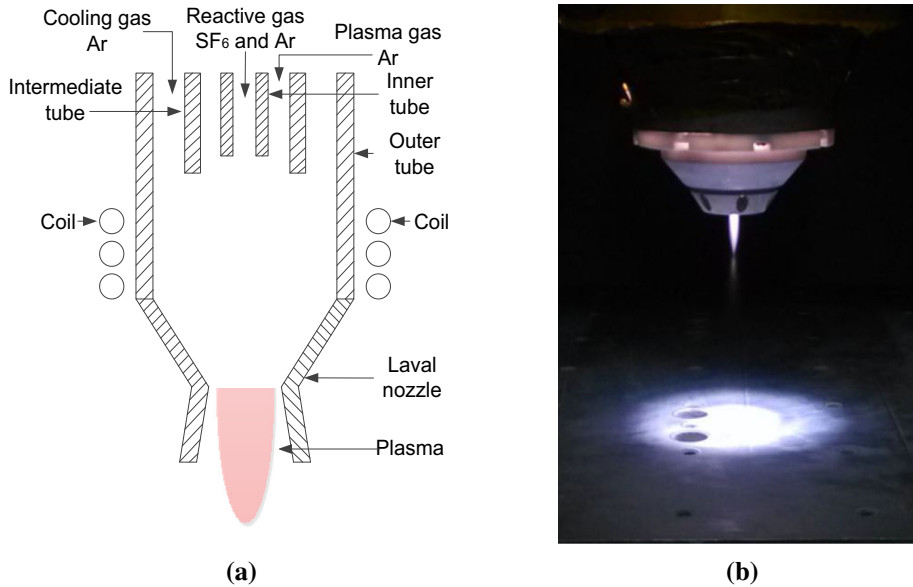
**Fig. 1** ICP source: **a** plasma source structure and **b** plasma beam

is connected to the Laval nozzle. Figure 1b shows the plasma source in operation with plasma beam that is produced. The experimental method to obtain the removal function is based on the plasma beam etched interferometric footprint to evaluate this removal function. To improve the evaluated accuracy, two approaches are usually employed. One is used to etch four to eight footprints on an optical planar surface, then to evaluate the removal function with the average of these footprints. In the other approach, the plasma beam scans linearly on planar optical surface with a velocity and constant plasma source parameters, which etches a trench on planar optical surface. The transverse material removal profile along its trench can be very closely approximated as the removal function. With the above two methods, the linearly scanning approach is more suitable for evaluating the removal function since it includes more information about the thermal effect. So, this paper adopts this method to accurately extract and describe the characteristics of the removal function.

To evaluate the ICP etching behavior for fused silica, we first have done some test experiments with 5 mm and 8 mm, two different etching target distances (stand-off interval between bottom of Laval nozzle and figuring surface) on 100 mm square planar fused silica samples with thickness of 10 mm, respectively. The experimental parameters are 1200 W RF power with 27.12 MHz frequency, 15 sccm CF_6 as reactive gas. The plasma carrier gas in both cases is Ar with a flow rate of 35 sccm in the inner tube, 1.12 slm in the intermediate tube and 16.8 slm in the outer tube. In addition, the experimental parameters can be formulated according to the experimental requirements. To obtain the material removal rate of the removal function at different scanning velocities, the experiments were carried out using a segmented variable velocities scanning test. It can be used to distinguish and extract a certain scanned trench segment from the plasma beam etched trenches, as shown in Fig. 2.
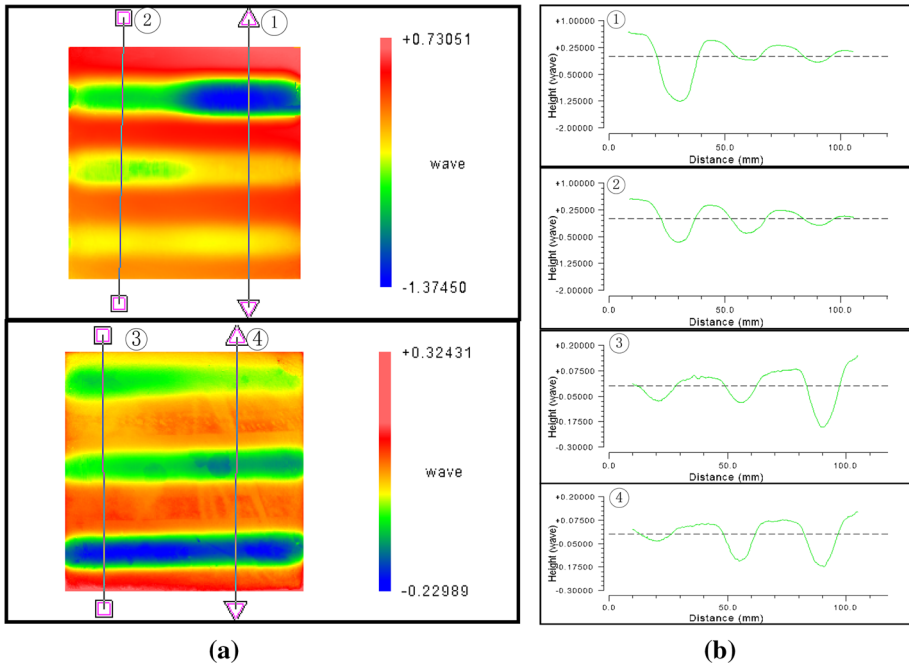
Fig. 2 Segmented variable velocities scanning test results: **a** trenches for different scanning velocities and **b** cross-sectional shape of trenches

Figure 2 shows the plasma beam etched trenches for different scanning velocities with 5 mm target distance on the two fused silica work-pieces with a size of 100 mm × 100 mm × 10 mm. Meantime, the etched trenches are divided into 4 trench segments; each of trench segments is etched by the plasma beam with 3 kinds of scanning velocities. In Fig. 2a, from top to bottom, the scanning velocities are 200, 500, 600 mm/min for the 1st trench segment, 300, 400, 700 mm/min for the 2nd trench segment, 1600, 1300, 800 mm/min for 3rd trench segment, 2000, 1100, 900 mm/min for the 4th trench
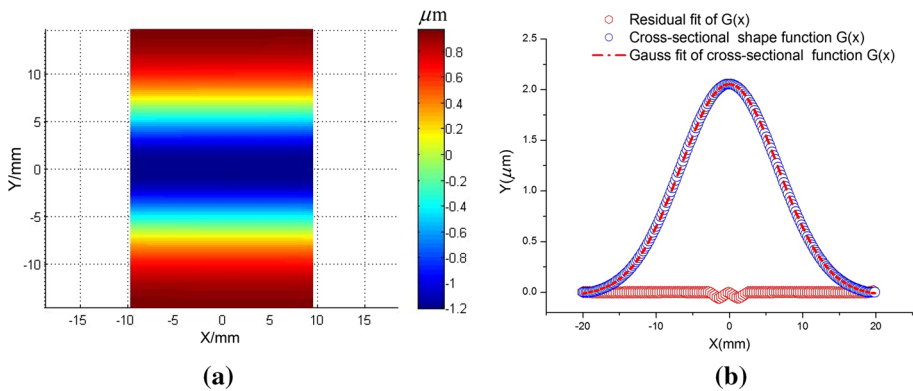
Fig. 3 Material removal footprint at 200 mm/min: **a** trench of material removal footprint and **b** cross-sectional shape of the trench

segment, respectively. Figure 3a shows the segment of the 1st trench achieved with 200 mm/min. Its material removal footprint was extracted by Metropro-zygo software. Figure 3b shows the cross-sectional shape of the trench and Gaussian-type fitting. The cross-sectional shape of the trench's mathematical fitting formula can be written as:

$$G(x) = 2.023 \cdot e^{-\frac{x^2}{2 \times 6.49^2}} \tag{1}$$

Since the plasma beam has a symmetrical distribution in the X and Y directions, the removal function at 200 mm/min can be given by Eq. (2). This removal function is a typical Gaussian-type distribution, as shown in Fig. 4.

$$R(x, y) = 24.871 \cdot e^{-\frac{x^2 + y^2}{2 \times 6.49^2}} \tag{2}$$

Consequently, the experimental model of removal function at a certain scanning velocity can be described by the general Eq. (3).

$$R(x, y) = A \cdot e^{-\frac{x^2 + y^2}{2 \times \sigma^2}} \tag{3}$$

where A is the peak removal rate, σ is the parameter of Gaussian function.

    Since the material removal mechanism of ICP etching is mainly a chemical reaction, the temperature has a great influence on the reactive etching rate. Accordingly, the relationships between the material removal rate, the peak temperature (maximum temperature on work-piece surface produced by the plasma beam) and dwell time (reciprocal of scanning velocity) are the key factors to be considered in developing an accurate experimental model of the removal function. Figure 5 shows the temperature distribution for a scanning speed of 600 mm/min with 5 mm target distance, and the peak temperature is about 440 °C.

    Figure 6 shows the material removal rate at different dwell time (or scanning velocity) with 5, 8 mm target distance respectively. For example for 5 mm target distance, the material removal rates increase from 1.89 mm³/min at 0.03 s/mm to 6.05 mm³/min at 0.3 s/mm. The target distance influence is also obvious with the material removal rate at 5 mm target distance is about 1.25 times that at 8 mm target distance. All of these changes are non-linear. By means of statistical analysis and fitting, it is found out that the material removal rate variation versus dwell time can be described by an exponential distribution.

Fig. 4 Experimental model of removal function at 200 mm/min
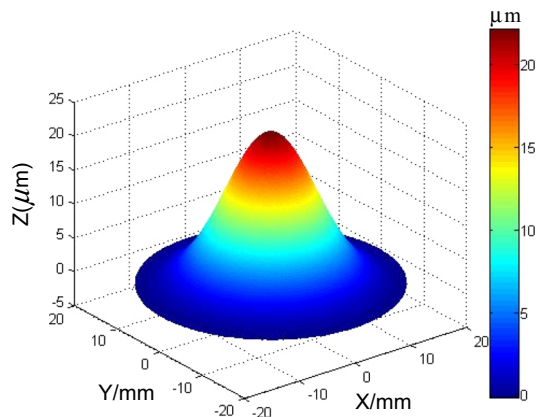
**Fig. 5** Scanning temperature distribution
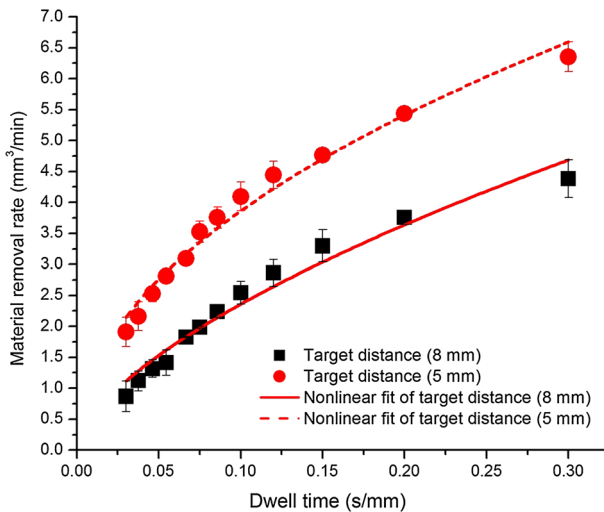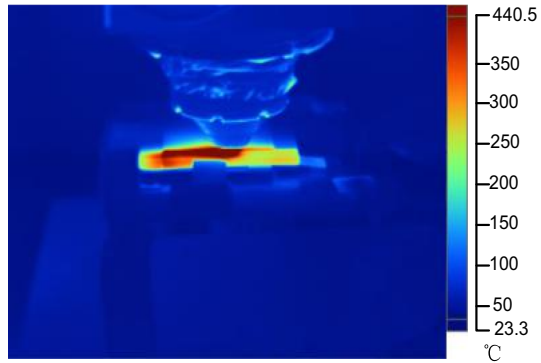
Fig. 6 Material removal rate versus dwell time

Equations (4) and (5) are the fitted exponential distribution formula at 5 mm and 8 mm target distances with the fit quality of 0.9963 and 0.9953 respectively, which indicates these equations were well fitted to the measured data. The non-linearity of the material removal rate is described by:

$$f(t) = 11.81621 \cdot t^{0.55641} \tag{4}$$

$$f(t) = 9.99091 \cdot t^{0.57662} \tag{5}$$

The material removal rate described above is the volume removal rate. Now we simply discuss the peak removal rate of the plasma beam. Figure 7 shows the variety of peak removal rate versus dwell time with 5, 8 mm target distance respectively. It is clear that peak removal rate also has a non-linear exponential dependence on dwell time. Figure 8 shows the steeply exponential variation of the peak removal rate with peak temperature, which verifies that the influence of surface temperature on peak removal rate is exponential.
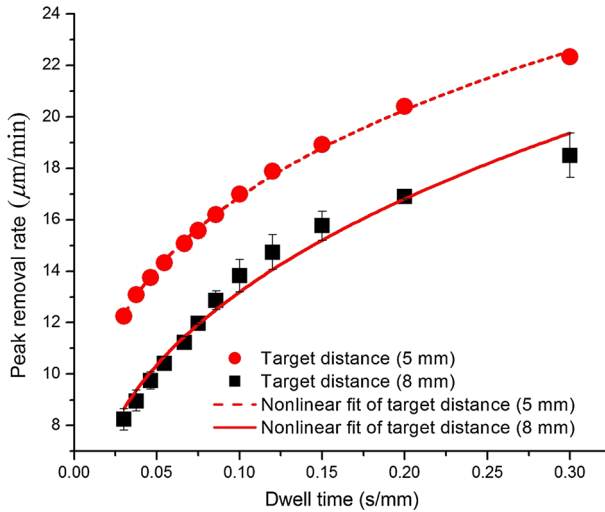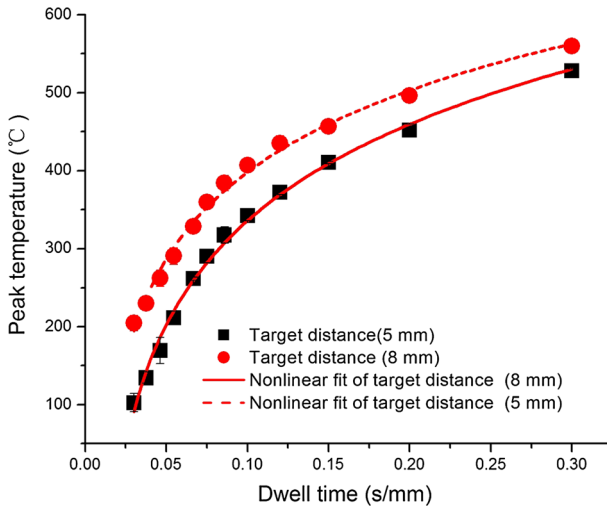
Fig. 7 Peak removal rate versus dwell time
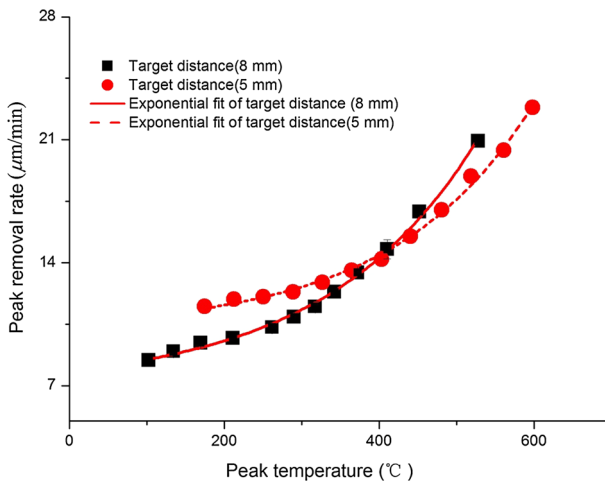
Fig. 8 Peak removal rate versus peak temperature

In order to estimate the thermal effect of the time-varying non-linearity, the dependence of peak temperature on dwell time is shown in Fig. 9. The peak temperature increases from 174 °C at 0.03 s/mm to 598 °C at 0.3 s/mm because of the low thermal diffusivity of the fused silica work-piece. This indicates that the surface temperature is significantly influenced by the plasma thermal flux onto the work-piece surface. Meanwhile, the heating throughout the dwell time causes the different chemical reaction rate. The relationship between peak temperature and dwell time is consistent with that of the material removal rate, which confirms that the time-varying non-linearity of material removal rate is caused by the local heating. Moreover, the peak temperature for 5 mm target distance is higher by about 70 °C than that for 8 mm target distance, which further intensifies the local thermal effect on the chemical reaction rate.

Fig. 9 Peak temperature versus dwell time

Accordingly, the time-varying non-linearity of material removal rate can be described as:

$$f(t) = \alpha \cdot t^{\wedge k} \tag{6}$$

where α is the non-linear coefficient of material removal rate, k is a non-linearity constant, t is the dwell time ($t = 1/v$, v: scanning velocity).

From the above statistical analysis of the experimental results, the time-varying non-linearity between material removal rate and dwell time is consistent with that of peak removal rate. In order to describe the removal function accurately, an experimental model of the removal function that considers the time-varying non-linearity is established, and is given in Eq. (7).

$$R(x, y, t) = \frac{\alpha \cdot t^{\wedge k}}{2\pi\sigma^2} e^{-\frac{x^2 + y^2}{2 \times \sigma^2}} = \frac{\alpha \cdot t^{\wedge k}}{2\pi A\sigma^2} R(x, y) \tag{7}$$

where α is the non-linear coefficient of material removal rate, k is a non-linearity constant, t is the dwell time, A is the peak removal rate, σ is the parameter of Gaussian function.

Calculation and Compensation for Dwell Time

Dwell Time Calculation

The dwell time is the input control for optical elements surface figuring, so accurate calculation of the dwell time has always been a key issue. Theoretically, the removed material $E(x, y)$ [23] in one iteration can be represented by a convolution of the removal function $R(x, y)$ and the dwell time $T(x, y)$, given as follows:

$$E(x, y) = R(x, y) \otimes T(x, y) = \int_{-\infty}^{+\infty} \int_{-\infty}^{+\infty} R(x - x', y - y') T(x', y') dx' dy' \tag{8}$$

Herein, it is assumed that the initial surface error $E_0(x, y)$ can be completely removed during the surface figuring process, where the actual removal material $E(x, y)$ after the iterative calculation is expected to approach the ideally removed material $E_0(x, y)$ as nearly as possible. Then, the convolution operation of the Fourier transform of Eq. (8) is done using the known removal material $E_0(x, y)$ and the removal function $R(x, y)$, Then the iterative calculation are utilized to reach the final required residual surface precision for calculating the dwell time $T(x, y)$.

In the surface figuring process, the dwell time usually can be expressed as Eq. (9) by the digital convolution operation. Therefore, the calculation of dwell time can be transformed into an iterative calculation of linear equations, avoiding negative values of dwell time, using so-called iterative operations.

$$E(x_m, y_n) = \sum_{i=11}^{M} \sum_{j=1}^{N} R\left(x_m - x_i', y_n - y_j'\right) T\left(x_i', y_j'\right) \tag{9}$$

where $E(x_m, y_n)$ is the removed material at the point (x_m, y_n), $R(x_m - x_i', y_n - y_j')$ is the removed material at the point (x_m, y_n) when the plasma beam is at the point (x_m, y_n), and $T(x_i', y_j')$ is the dwell time at the point (x_m, y_n) ($m = 1, 2\ldots M, n = 1, 2\ldots N, i = 1, 2\ldots M, j = 1, 2\ldots N$).

Dwell Time Non-linear Compensation

The dwell time can be calculated through the iterative application of Eq. (9) in the case of linear material removal conditions. However, this condition can not satisfy the requirement of the ICP surface figuring since its chemical etching rate is affected by the reactive temperature. To solve this problem, an Arrhenius-type model is formulated in Eq. (10), which considers the chemical reactive energy, temperature and so on [6].

$$MRR = C \cdot n_F \cdot \exp\left(-\frac{E_a}{RT}\right) \tag{10}$$

where MRR is the material removal rate, n_F is the fluorine concentration, E_a is the active reaction energy, R is the gas constant, C is a material constant and T is the reactive temperature.

The considerable thermal effect on material removal rate requires the introduction of compensatory techniques in order to secure better convergence of surface figuring process [6, 22, 24]. Hence, an overall time-varying non-linearity of material removal rate is to be expected. This can be formulated in Eq. (11) as in Johannes Meister et al. [6] and M. Castelli et al. [22].

$$E(x_m, y_n) = \sum_{i=11}^{M} \sum_{j=1}^{N} R\left(x_m - x_i', y_n - y_j'\right) \cdot f\left[T\left(x_i', y_j'\right)\right] \tag{11}$$

According to the experimental model of removal function described in Eq. (7), the removal function $R(x, y, t)$ at the dwell time $T(x', y')$ can be written as:

$$R(x, y, t) = \frac{\alpha \cdot [T(x', y')]^{\wedge k}}{2\pi A \sigma^2} R(x, y) = R[x, y, T(x', y')] \tag{12}$$

The convolution of the removal function and dwell time can be written as:

$$E(x_m, y_n) = \sum_{i=11}^{M} \sum_{j=1}^{N} R\left[x_m - x_i', y_n - y_j', T\left(x_i', y_j'\right)\right] \cdot T\left(x_i', y_j'\right) \tag{13}$$

Therefore, assuming $T(x_i', y_j')$ is basic dwell time at a certain removal function, the compensated dwell time $T_0(x_i', y_j')$ can be written as:

$$T_0\left(x_i', y_j'\right) = \frac{2\pi A\sigma^2}{\alpha \cdot [T(x', y')]^{\wedge k}} T\left(x_i', y_j'\right) = \frac{2\pi A\sigma^2 \cdot \left[T\left(x_i', y_j'\right)\right]^{\wedge(1-k)}}{\alpha} \tag{14}$$

As shown in Fig. 10, when the dwell time is calculated by iterative operations, the actual material removal rate with time-varying non-linearity cannot be directly considered in the process. The surface figuring dwell time cannot be obtained accurately according to iterative operations through Eq. (9). Consequently, the basic dwell time should be calculated by iterative operations. Then, the time-varying non-linearity is compensated using the basic dwell time.

To achieve a convenient method to calculate and compensate dwell time, in this paper, an algorithm based on NPIM is proposed. Pulsed iterative operations, a classic algorithm based on iterative operations, are used to calculate basic dwell time. NPIM is used to calculate and compensate the basic dwell time considering the time-varying non-linearity. In this way, the more accurate dwell time can be obtained as long as the figuring removal function is suitably selected. This algorithm can allow a high precious material removal by means of improving figuring efficiency and achieve the high surface error convergence. The specific steps in the algorithm may be stated as follows.

Step (1) Calculate the basic dwell time

(a) Take an appropriate removal function R_0 and the strength of its removal function M_0 to calculate the removal material H based on Eq. (9). (b) Calculate the initial basic dwell
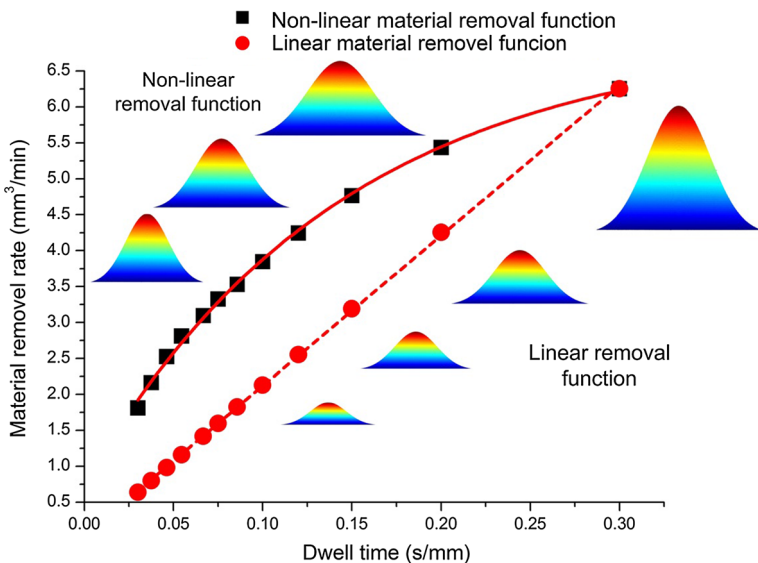
Fig. 10 Relationship between material removal rate of removal function and dwell time

time $T_i = H/M_0$ and the residual error $E_i = H - T_i * R_0$ ($i = 0$). (c) Calculate the correction parameter of dwell time $\Delta_i = E_i/M_0$. (d) Correct the dwell time $T_{i+1} = T_i + \Delta_i$. (e) Test non-negativity for the dwell time T_{i+1}: if there is a negative element in T_{i+1}, set it to zero. (f) Calculate the residual error $E_{i+1} = H - T_{i+1} * R_0$. (g) Judge whether the dwell time T_{i+1} and the residual error E_{i+1} satisfy the requirements. If satisfied, end the calculation and go to the step 2. Otherwise, let $i = i + 1$, and return to step 1 (c).

Step (2) Calculate the compensated dwell time

(a) Based on Eqs. (12), (13) and (14), apply the non-linear removal function R_j shown in Fig. 10 and the strength of its removal function $M_j * (\alpha * (T_{i+1})^{\wedge k})$ ($j = 0$) to correct the removal function R_0. When the dwell time T_{i+1} is corresponding to T_j, place $T_j = T_{i+1}$. (b) Calculate the residual error $E_{i+1} = H - T_j * R_j$. (c) Calculate the correction parameter of dwell time $\Delta_i = E_{i+1}/M_j$. (d) Correct the dwell time $T_{i+2} = T_{i+1} + \Delta_{i+1}$. (e) Test non-negativity for the dwell time T_{i+2}: if there is a negative element in T_{i+2}, set it to zero. (f) Calculate the residual error $E_{i+2} = H - T_{i+2} * R_j$. (g) Judge whether the dwell time T_{i+2} and the residual error E_{i+2} satisfy the requirements. If satisfied, end the calculation, and set $T_{j+1} = T_{i+2}$, then go to step 3. Otherwise, let $i = i+1$, and return to step 2 (c).

Step (3) Judge whether the convergence conditions are satisfied

(a) Calculate the dwell time residual error $\Delta T_j = T_{j+1} - T_j$. (b) Judge whether the dwell time residual error ΔT_j satisfies the requirements. If satisfied, Finish the calculation, and output the dwell time T_{j+1}. Otherwise, let $j = j + 1$, and return to step 2 until the parameter estimates converge to the requirements.

To check this algorithm, a simulation was done with the removal function at 0.3 s/mm on the fused silica work-piece with a size of 100 mm × 100 mm × 10 mm. The initial surface error is shown in Fig. 11a, and the simulated processed surface is shown in Fig. 11b. The PV is reduced from 4.556 λ to 0.776 λ and the RMS is reduced from 1.161 λ to 0.032 λ. The dwell time calculated by the pulsed iterative operations is shown in Fig. 11c. The total processing time is about 22.6 min. The compensated time is shown in Fig. 11d, and the time is about 9.4 min. Then, the final compensated dwell time for the numerical control machining code is shown in Fig. 11e. The processing time is reduced to about 13.2 min. As shown in Fig. 11f, the convergent curve shows that the algorithm can calculate and compensate the dwell time accurately and efficiently.

Figuring Experiments and Discussion

Figuring Experiments

To investigate the surface figuring capability of the algorithm, experiments were done on two polished fused silica planar surfaces with 100 mm×100 mm square, thickness of 10 mm. These two surfaces were carefully polished in a preparation process to yield similar original surface characteristics as shown in Fig. 13a, c. The low frequency errors of the surfaces were relatively abundant. The surface figuring experiments were carried out on a self-developed ICP machining system. The experimental parameters were RF power of 1200 W with 27.12 MHz frequency, 5 mm target distance, 35 sccm Ar and 15 sccm SF_6 in the inner tube, 1.12 slm Ar in the intermediate tube, 16.8 slm Ar in the outer tube.

In these experiments, the influence of tool-paths is considered. Figure 12 gives two kinds of tool-paths, reversed staggered raster path and reversed staggered raster nested
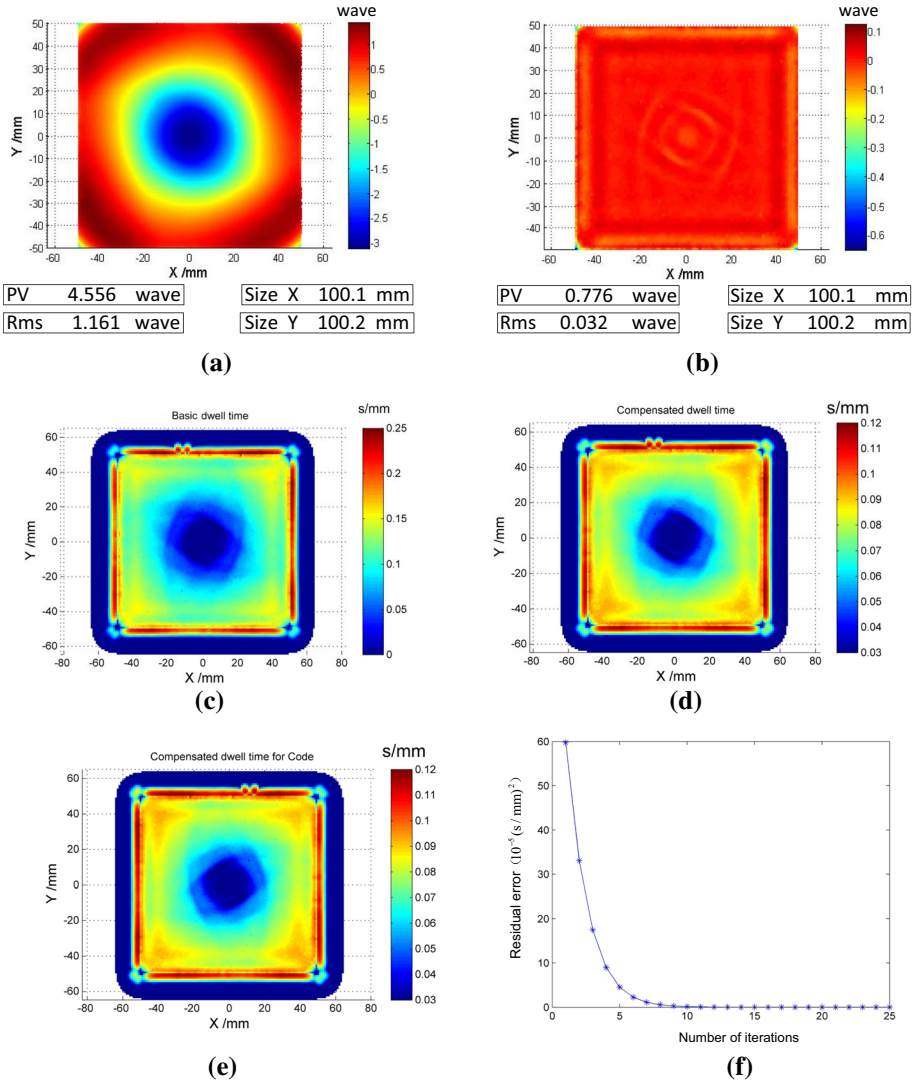
Fig. 11 Simulation results: **a** initial surface error, **b** residual errors, **c** basic dwell time, **d** compensated dwell time, **e** compensated dwell time for code and **f** convergence curve of the algorithm

path. The simulated and experimental results in both cases demonstrate that the tool-path influence is not obvious, so the reversed staggered raster with 3 mm staggering was applied in the surface figuring experiment.

Within these surfaces figuring experiments, the figuring process was intentionally divided into two groups to investigate surface error evolution. One was carried out by using the basic dwell time, which was calculated directly by the algorithm of pulsed iterative operations with the appropriate removal function, which is called uncompensated surface figuring. The other was applied to the compensated dwell time, which is called compensated surface figuring. Consequently, for the uncompensated surface figuring experiment,
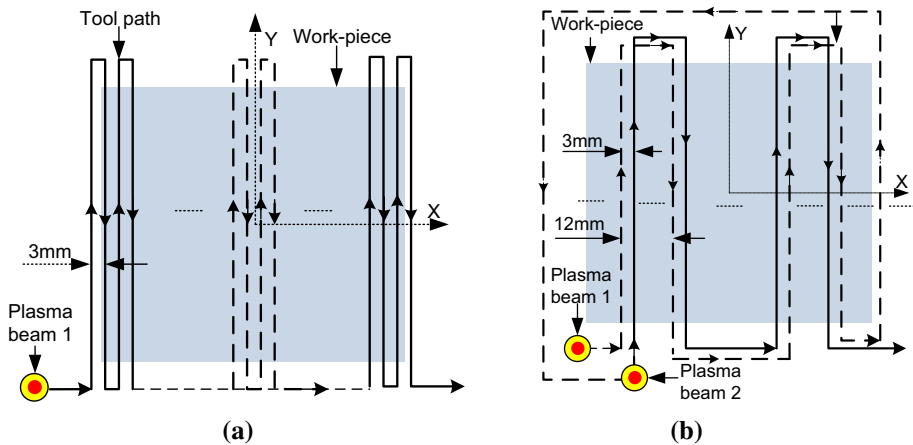
Fig. 12 Tool-paths: **a** reversed staggered raster path and **b** reversed staggered raster nested path

the processed surface shape is changed from the initial concave surface shape shown in Fig. 13a to the convex surface shown in Fig. 13b. The related dwell time is shown in Fig. 11c. The PV changed from 4.716 λ to 4.221 λ and the contour errors slightly increased from 1.152 λ RMS to 1.283 λ. The result of the compensated surface figuring experiment is shown in Fig. 13c, d, and Fig. 11e is the related dwell time. The PV converged from 4.556 λ to 0.839 λ and the contour error decreases from 1.161 λ RMS to 0.068 λ RMS, which confirmed the simulation results and achieved highly efficient figuring with rapid convergence of the surface error for a fused silica work-piece.

PSD Discussion

For further evolution of the surface error at different frequencies, we take the PSD functions of the images from the experimental surface figuring results (Fig. 13a–d) for comparison. As shown in Fig. 14, the PSD curves a, b, c and d correspond to Fig. 13a, b, c and d respectively. Figure 14 shows that the low spatial frequency errors within [0.01 mm^{-1}, 0.04 mm^{-1}] interval range are effectively eliminated by the compensated surface figuring. On the other hand, the spatial frequency errors within the same range are not obviously corrected obviously by the uncompensated surface figuring. The trend of the PSD curves also demonstrates that the initially existing high-slope errors are rapidly smoothed by the compensated surface figuring. Additionally, the spatial frequency errors within the [0.04, 0.972 mm^{-1}] interval range are also slightly corrected. The spatial frequency errors within the [0.972, 4.289 mm^{-1}] interval range are clearly increased by the compensated surface figuring, while the spatial frequency errors are not increased after the uncompensated surface figuring. The material removal depth of the uncompensated surface figuring is deeper than the compensated one, which causes non-convergence of the sample's surface shape, but removes the subsurface damage. In this process, due to the preprocessing of polishing, lapping and grinding, damage is imparted so that it can propagate below the surface. This figuring process exposes the subsurface damage along the material removal depth. So the spatial frequency errors in these ranges can be gradually exposed and then gradually smoothed along the material removal depth, as is shown in Fig. 15. It can be seen
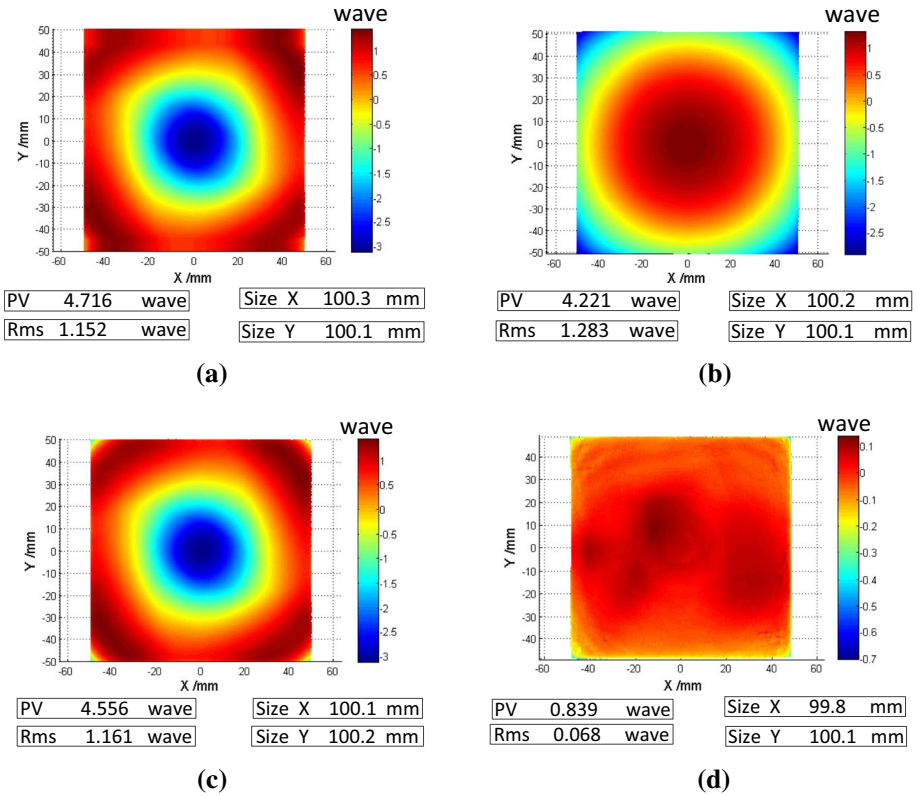
Fig. 13 Experimental surface figuring results: **a** initial surface I (surface error for uncompensated surface figuring), **b** surface error after uncompensated surface figuring, **c** initial surface II (surface error for compensated surface figuring) and **d** surface error after compensated surface figuring

**Fig. 14** Evolution of PSD during ICP surface figuring process
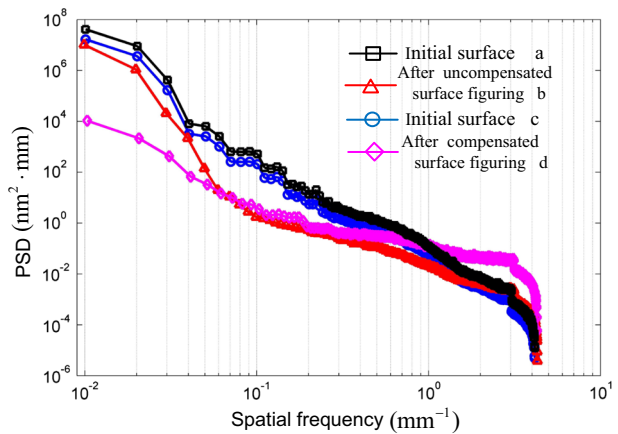
that the PSD analysis further verifies that the compensated surface figuring can acquire rapid convergence for surface error and good surface quality.

Conclusion

In this paper, to compensate the time-varying non-linearity of material removal rate caused by the thermal effect during the ICP surface figuring process, an algorithm based on NPIM is proposed for calculating and compensating the time-varying non-linearity to dwell time. This algorithm provides a convenient dwell time compensation approach for fused silica surface figuring. The main conclusions are as follows:

1. The method of segmented variable velocity scanning testing by plasma beam etching is applied to analyze the time-varying non-linearity of material removal rate of ICP etching. The analysis validates that the thermal accumulation on the surface is the main factor which influences the time-varying non-linearity of removal function. Then the experimental model of removal function is established considering the time-varying non-linearity.

2. According to the experimental model of the removal function, the NPIM only needs to apply the time-varying non-linearity to the nested pulsed iterative calculation, which is more convenient to accurately calculate and compensate the time-varying non-
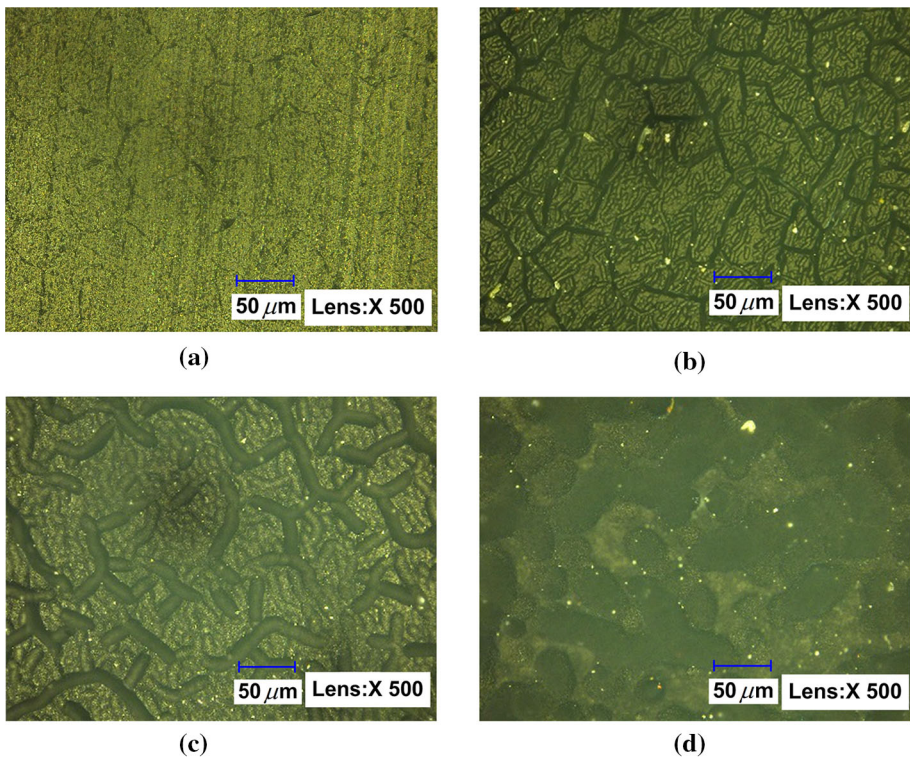
Fig. 15 Subsurface damage variation during material removal depth: **a** initial surface, **b** 1.2 μm removed in depth, **c** 2.6 μm removed in depth, **d** 4.8 μm removed in depth without subsurface damage defects

linearity to dwell time for the ICP fused silica surface figuring. The experimental figuring dwell time is reduced from 22.6 min down to 13.2 min by compensated surface figuring, so this algorithm could improve the calculated accuracy of the dwell time. The surface error converges from 4.556 λ PV to 0.839 λ PV, and the convergence ratio is about 5.43, which demonstrates the rapid convergence for ICP plasma surface figuring. All the above simulations and experiments confirm that the algorithm is applicable.

3. The PSD analysis results show that this proposed algorithm clearly controls the low and middle spatial frequency errors, which demonstrates its strong corrective capability for surface contour errors.

References

1. Li N, Wang B, Jin H (2014) Harbin Inst Technol 21(5):124–128
2. Wang Z, Wu Y, Dai Y (2007) Aviat Precis Manuf Technol 43(5):1–5
3. Nie X, Li S, Dai Y, Song C (2013) Proc SPIE Int Soc Opt Eng 8786(22):11306–11312
4. Shen J, Liu S, Yi K, He H, Shao J, Fan Z (2005) Optik Int J Light Electron Opt 116(6):288–294
5. Wang Y, Hang L, Hu M (2008) Surf Technol 37(1):51–53
6. Meister J, Arnold T (2011) Plasma Chem Plasma Process 31:91–107
7. Mori Y, Yamamura K, Sano Y (2000) Rev Sci Instrum 71(12):4620–4626
8. Takino H, Yamamura K, Sano Y, Mori Y (2010) Appl Opt 49:4434–4440
9. Eichentopf I-M, Böhm G, Meister J, Arnold T (2010) Plasma Process Polym 6(S10):S204–S208
10. Arnold T, Böhm G, Fechner R, Meister J, Nickel A, Frost F, Hansel T, Schindler A (2010) Nucl Instrum Methods Phys Res A 616:147–156
11. Arnold T, Böhm G (2012) Precis Eng 36(4):546–553
12. Eichentopf I-M, Böhm G, Arnold T (2011) Surf Coat Technol 205(205):S430–S434
13. Fanara C, Shore P, Nicholls J-R, Lyford N, Sommer P, Fiske P (2006) SPIE Astron Telesc Instrum Int Soc Opt Photonics 10:933–939
14. Jourdain R, Castelli M, Shore P, Sommer P, Proscia D (2013) Prod Eng Res Devel 7:665–673
15. Zhang J, Wang B, Dong S (2008) Int J Precis Eng Manuf 9(2):39–43
16. Jia G, Li B, Zhang J (2016) Mater Sci Forum 878:83–88
17. Shi B, Dai Y, Xie X, Li S, Zhou L (2016) Plasma Chem Plasma Process 36(3):1–10
18. Shi B, Xie X, Dai Y, Liao C (2014) Proc SPIE 9281:928104
19. Greenfield S, Jones I (1964) Analyst 89(1064):713–720
20. Castelli M, Jourdain R, Morantz P, Shore P (2012) Proc SPIE Int Soc Opt Eng 8450:34
21. Wendt R, Fassel V (1965) Anal Chem 37(7):920–922
22. Castelli M, Jourdain R, Morantz P, Shore P (2012) Precis Eng 36(3):467–476
23. Liao W, Dai Y, Xie X (2014) Opt Eng 53(9):095101
24. Arnold T, Böhm G, Paetzelt H (2016) Nonconventional ultra-precision manufacturing of ULE mirror surfaces using atmospheric reactive plasma jets. In: SPIE astronomical telescopes and instrumentation, p 99123N